

RESEARCH

Open Access



# GAS6 as a potential target to alleviate neuroinflammation during Japanese encephalitis in mouse models

Peiyu Bian<sup>1†</sup>, Haijun Zhang<sup>2†</sup>, Chuantao Ye<sup>3†</sup>, Chuanyu Luo<sup>4</sup>, Hong Jiang<sup>3</sup>, Yuan Wang<sup>5</sup>, Yangchao Dong<sup>5</sup>, Jing Yang<sup>5</sup>, Fanglin Zhang<sup>5</sup>, Xiaoming Wang<sup>1</sup>, Ying Zhang<sup>3\*</sup>, Zhansheng Jia<sup>6\*</sup> and Yingfeng Lei<sup>5\*</sup>

## Abstract

Viral encephalitis is characterized by inflammation of the brain parenchyma caused by a variety of viruses, among which the Japanese encephalitis (JE) virus (JEV) is a typical representative arbovirus. Neuronal death, neuroinflammation, and breakdown of the blood brain barrier (BBB) constitute vicious circles of JE progression. Currently, there is no effective therapy to prevent this damage. Growth arrest specific gene 6 (GAS6) is a secreted growth factor that binds to the TYRO3, AXL, and MERTK (TAM) family of receptor tyrosine kinases and has been demonstrated to participate in neuroprotection and suppression of inflammation in many central nervous system (CNS) diseases which has great potential for JE intervention. In this study, we found that GAS6 expression in the brain was decreased and was reversely correlated with viral load and neuronal loss. Mice with GAS6/TAM signalling deficiency showed higher mortality and accelerated neuroinflammation during peripheral JEV infection, accompanied by BBB breakdown. GAS6 directly promoted the expression of tight junction proteins in bEnd.3 cells and strengthened BBB integrity, partly via AXL. Mice administered GAS6 were more resistant to JEV infection due to increased BBB integrity, as well as decreased viral load and neuroinflammation. Thus, targeted GAS6 delivery may represent a strategy for the prevention and treatment of JE especially in patients with impaired BBB.

**Keywords** Japanese encephalitis virus, GAS6, Blood brain barrier, Neuroinflammation, GAS6 overexpression

<sup>†</sup>Peiyu Bian, Haijun Zhang and Chuantao Ye contributed equally to this work.

\*Correspondence:

Ying Zhang  
zyfmmu@hotmail.com  
Zhansheng Jia  
jjazsh@fmmu.edu.cn  
Yingfeng Lei  
yflei@fmmu.edu.cn

<sup>1</sup>Department of Geriatrics, Xijing Hospital, Air Force Medical University, Xi'an 710027, China

<sup>2</sup>Xijing 986 Hospital, Air Force Medical University, Xi'an 710054, China

<sup>3</sup>Department of Infectious Diseases, Tangdu Hospital, Air Force Medical University, Xi'an 710038, China

<sup>4</sup>Norinco General Hospital, Xi'an 710065, China

<sup>5</sup>Department of Microbiology, School of Preclinical Medicine, Air Force Medical University, Xi'an 710032, China

<sup>6</sup>Department of Infectious Diseases, Xi'an International Medical Center Hospital, Xi'an 710100, China



## Background

Viral encephalitis is characterized by acute fever, headache, and damage to the brain parenchyma leading to changes in mental status and seizures. It can be caused by more than 100 types of viruses, including arbovirus, tick-borne viruses, herpes encephalitis viruses, and enteroviruses. Japanese encephalitis virus (JEV) is the leading cause of viral encephalitis in Asia and is a typical representative of arbovirus. Before the launch of JEV vaccine, children were the main victims because of the immaturity of the blood-brain barrier (BBB) [1]. However, the number of middle-aged and elderly patients with JE is increasing, especially those with cerebrovascular diseases [2]. There is no effective treatment for JE but supportive therapies. The mortality rate of JE patients can reach approximately 30%, and even survivors are often accompanied with severe neuropsychiatric disorders [1]. After entering the central nervous system (CNS), JEV causes extensive neuronal damage directly and indirectly through immune-mediated inflammation, including glial activation, inflammatory cell infiltration, and damage-associated molecule patterns (DAMPs) production [3]. The BBB is a portal for viral entry, and increased neuroinflammation exacerbates BBB breakdown, allowing more inflammatory mediators to enter the CNS [4]. Therefore, blocking the vicious circle of neuroinflammation is a promising therapeutic strategy for the treatment of viral encephalitis.

Growth arrest specific gene 6 (GAS6) is a secreted growth factor that binds to the TYRO3, AXL, and MERTK (TAM) family of receptor tyrosine kinases [5]. GAS6 is an anti-inflammatory, neuroprotective, and promyelinating agent. AXL, the receptor with the highest affinity for gas6, has been shown to alleviate neuroinflammation and delay JE progression in mice during JEV infection [6]. Our group found that AXL-deleted neurons promoted JEV propagation furtherly by dampening innate immunity [7]. As the sole ligand of AXL, gas6 promoted AXL expression and activation of AXL [5]. Supplementation with GAS6 protected axons from damage during experimental autoimmune encephalomyelitis [8] and enhanced the tight-junction barriers in the intestinal epithelium to prevent *K. pneumoniae* from translocating into livers and lungs [9]. Because neuroinflammation and BBB breakdown are the main characteristics of JE, there is an urgent need to explore the effect of GAS6 on JE progression.

In this study, we found that morbidity and mortality increased significantly in gas6 knockout (KO) as well as AXL/MERTK-deleted mice after peripheral JEV injection. Additionally, we observed an increase in the destructive breakdown of the BBB and vigorous neuroinflammation in GAS6/TAM blocked mice during JEV infection. Recombinant AAV-gas6 (rAAV-gas6)

was injected into the lateral ventricle to increase GAS6 expression in the brain, and mice overexpressing GAS6 showed more resistance to JEV infection and decreased neuroinflammation compared to controls. Thus, GAS6/TAM signalling may represent a therapeutic target for preventing JEV entry into brains and alleviating neuroinflammation, especially in elderly patients with cerebrovascular diseases.

## Materials and methods

### Ethics statement

All animal experiments were reviewed and approved by the Animal Care and Use Committee of the Laboratory Animal Center, Air Force Medical University. The number of Animal Experimental Ethical Inspection is 20,160,112. And all experiments were carried out complying with recommendations in the Guide for the Care and Use of Laboratory Animals.

### Mice

The C57BL/6 mice were purchased from Laboratory Animal Center, Air Force Medical University. The C57BL/6-GAS6<sup>+/-</sup> mice were constructed via CRISPR CAS9 in Cyagen Biosciences Company (China). AXL<sup>-/-</sup> and AXL/MERTK<sup>-/-</sup> mice were kindly gifted from Professor Daishu Han (Institute of Basic Medical Sciences, Peking Union Medical College-Chinese Academy of Medical Sciences) and were maintained in a specific pathogen-free (SPF) facility. Toe DNA was extracted from new-born mice and amplified using PrimeStar (Takara, Bio, Shiga, Japan). The products were analysed using agarose gel electrophoresis to screen for wild-type (WT), GAS6<sup>+/-</sup>, GAS6<sup>-/-</sup>, AXL<sup>+/-</sup>, AXL<sup>-/-</sup>, MERTK<sup>-/-</sup>, and AXL/MERTK<sup>-/-</sup> descendants. WT and AXL<sup>-/-</sup>, GAS6<sup>-/-</sup>, MERTK<sup>-/-</sup>, or AXL/MERTK<sup>-/-</sup> mice (6–8 weeks) were infected with JEV 10<sup>5</sup> or 10<sup>6</sup> plaque forming unit (PFU) in 20  $\mu$ l phosphate buffered saline (PBS) through footpad injection or 100 PFU in 2  $\mu$ l via intracerebral injection. The weight, behaviour score (according to the Scoring Criteria described previously [10]) and deaths of each group were recorded daily at 16:00–17:00 for 20 days until all groups were totally stable.

### Virus and cells

The JEV P3 strain was propagated in the brains of 3-day-old inbred BALB/c sucking mice and titrated using conventional plaque forming assay. Brain microvascular endothelial cell line bEnd.3 cells, astrocyte cell line C8-D1A cells, neuroblast cell line neuro2a cells, and baby hamster kidney (BHK) and AAV-293 cells were purchased from American Type Culture Collection (ATCC) and cultured in DMEM (Gibco, Grand Island, NY, USA) containing 10% fetal bovine serum (FBS; Gibco, Grand

Island, NY, USA) and 1% penicillin streptomycin combination (PS).

### BBB permeability measurement

Mice were infected with JEV or PBS and BBB permeability was assessed at 3- and 5-days post infection (dpi). For qualitative detection, mice were intravenously injected with 100  $\mu$ l of Evans Blue (EB, Sigma, St. Louis, MO, USA) solution (2% in PBS). After 1 h, all injected mice were sacrificed and transcardially perfused with 40 ml of 1 $\times$ PBS. The whole brains were removed and photographed. For quantitative assay, sodium fluorescein (NaF; 0.1 g/ml, 100  $\mu$ l, Sigma, St. Louis, MO, USA) was administered intraperitoneally. After 30 min, the mice were anaesthetised and blood was collected via the eyeballs into EDTA-coated tubes. The mice were then perfused with 40 ml 1 $\times$ PBS through cardiac puncture, and the brains were harvested. Serum (100  $\mu$ l) was mixed with an equal volume of 15% trichloroacetic acid (TCA; Sangon, China). After centrifugation for 30 min at 10,000 g, 120  $\mu$ l of supernatant was mixed with 30  $\mu$ l of 5 M NaOH. Then, brain tissues were homogenised in cold 7.5% TCA (150  $\mu$ l per 100 mg tissues) and centrifuged for 30 min at 10,000 g before collecting the supernatant (120  $\mu$ l) and mixing with 30  $\mu$ l of 5 M NaOH. The fluorescence of the serum and brain samples was determined using a BioTek Spectrophotometer (Bio-Tek Instruments, Winooski, VT, USA) with excitation at 485 nm and emission at 530 nm. The leakage of NaF into the tissue was expressed as (fluorescence brains/ mg)/ (fluorescence sera/ ml of blood).

### Hematoxylin–eosin (H&E) and immunohistochemical (IHC) staining

At 3 and 5 dpi, mice were anaesthetised and perfused with 1 $\times$  PBS followed by 4% paraformaldehyde (PFA) for 30 min. The brain was removed, fixed in 4% PFA for 12 h, and then dehydrated in 30% sucrose. Tissue sections of 10- $\mu$ m thickness were prepared using a vibratome. Standard H&E and IHC staining were performed as previously reported [10]. For IHC, after fixing with 4% PFA and blocking with 3% BSA containing 0.1% Triton X-100, the slides were incubated with primary antibodies anti-ZO-1 (Thermo, USA), anti-CD31 (Abcam, USA), and anti-AXL (Abcam, USA) diluted with PBS containing 0.1% Triton X-100 and 1% BSA for 16 h (as shown in Supplementary Table). After washing, the sections were incubated with the corresponding secondary antibodies: FITC-anti-rabbit IgG, Cy3-anti-rabbit IgG, and Cy3-anti-goat IgG (Proteintech, China) for 1 h at room temperature. The nuclei were counterstained with 4',6-diamidino-2-phenylindole (DAPI; Thermo, USA), and coverslips were placed on the samples with 50% glycerol in PBS.

### Western blotting

Total protein from the brain of each mouse or bEnd.3 cells was extracted with radio immunoprecipitation assay lysis (RIPA) buffer (Thermo, Waltham, MA, USA) and quantified using a Protein Reagent Assay BCA Kit (Thermo, Waltham, MA, USA). Thirty micrograms of protein from each sample were loaded and electrophoresed on 12% SDS-PAGE gels and then transferred onto a polyvinylidene difluoride (PVDF) membrane (Millipore, Billerica, MA, USA). Subsequently, the membranes were blocked with 3% bovine serum albumin (BSA) at room temperature for 60 min, and then incubated with primary antibodies to occludin (Thermo, USA), JEV E protein (prepared in our lab), claudin5 (Abcam, USA), and GAPDH (Proteintech, China) (as shown in Supplementary Table) overnight at 4  $^{\circ}$ C. Secondary antibodies including DyLight 700-anti-rabbit IgG (BD Biosciences, Franklin Lakes, NJ, USA) and DyLight 800-anti-mouse IgG (BD Biosciences, Franklin Lakes, NJ, USA) for 2 h at room temperature. Finally, blotings were visualised using an Infrared Imaging System (Odyssey, LI-COR, NE Lincoln, USA).

### qRT-PCR

Total RNA from each whole brain was extracted with RNAfast1000 (PIONEER, China) and then reverse-transcribed using a PrimeScript RT reagent Kit (TaKaRa, Japan). All qRT-PCR experiments were performed using SYBR Green Real-Time PCR Master Mix (TaKaRa, Japan) according to the manufacturer's instructions. The primers used in this study are listed in the Supplementary Table.

### Plaque assay

BHK cells were seeded into 12-well plates at  $2 \times 10^5$ /well overnight. The supernatant were removed and cells were washed twice with 1 $\times$ PBS. After sterile filtration, serum samples (1:5 dilution in DMEM) from JEV infected mice at 1 and 3 dpi were added and incubated at 37 $^{\circ}$ C for 2 h. Then, the viral supernatant was changed to 2 ml overlay medium (100 ml: 25 ml 4 $\times$ DMEM, 50 ml 4% methylcellulose, 2 ml FBS, 23 ml ddH<sub>2</sub>O). After incubation for 5 days, the overlay media were removed and the wells were cleared with 1 $\times$  PBS. Next, 1 ml 4% PFA was added into wells and fixed for 30 min. Crystal violet dye was added at 2 ml per well for 15 min and washed with running tap water. Finally, plaques were counted and photographed.

### Construction of AXL-KO bEnd.3 cells

Lenti V2 carrying CRISPR-Cas9 system targeting mus AXL sequence (5' -CGGAACCCGTGACCCTACT CTGG -3') was constructed. bEnd.3 cells were seeded in 6-well plates at a density of  $2 \times 10^5$  cells/ well overnight. The recombinant lentivirus was added and incubated

at 37°C. Approximately 48 h later, cells were screened using puromycin (5 µg/ml) for 1 week and positive cells were kept with 10% FBS DMEM containing puromycin (1 µg/ml) and sent for AXL sequencing and immunofluorescence. Finally, the AXL-KO bEnd.3 cells were constructed.

### BBB construction in vitro and transendothelial permeability assay

Neuro2a cells were plated in lower wells of 0.4 µM Transwell 24-well plates (BD Biosciences; Corning), and C8-D1A cells ( $1 \times 10^5$  cells in 100 µl DMEM) were plated into lower side of inserts. After 4 h, AXL KO bEnd.3 and bEnd.3 cells ( $5 \times 10^4$  cells in 600 µl DMEM media) were plated into inserts and cultured until confluency and tight junctions were well established. The media were removed and viral supernatants from JEV infected brain homogenates were added to the lower wells. The recombinant protein GAS6 (100 nM, RD, USA) was added to the treated groups. The barrier function of the endothelial monolayers was measured as TEER using a Millicell ERS Ohmmeter with a probe (Millipore, Burlington, MA, USA; MERS00002). TEER readings were taken at baseline and calculated according to data = (readings-blank readings)/0.33 mm<sup>2</sup>.

### Construction of pAAV-gas6

The gas6 genome derived from mice was amplified and introduced into the restriction enzyme sites Bgl-II and Xho-I through PCR. The DNA fragment was ligated into a linearised plasmid vector pAAV-MCS digested with endonuclease BamH-I (1 µl) and Xho-I (1 µl) through the T4 ligation system and transformed into XL10-Gold ultracompetent cells. Positive clones were sequenced and cultured to obtain the recombinant pAAV-gas6 (rAAV-gas6).

### Production of rAAV-gas6 particles

Transfection was conducted when AAV-293 cells were approximately 70–80% confluent. Three plasmids (pAAV-gas6 or pAAV-GFP 10 µg, pAAV-RC 10 µg, and pHelper 20 µg in 2 ml DMEM) were mixed with transfection reagent LipoFectMAX (ABP Biosciences, USA) (120 µl in 2 ml DMEM). After 25 min, the mixture was added to AAV-293 cells at T75. After incubation for 6 h at 37 °C, the medium was changed into 10 ml fresh DMEM growth medium. About 66 h later, the cells and supernatants were harvested for concentration and purification of rAAV-gas6 particles. Virus particles in the supernatant were deposited through centrifugation at 160,000 g for 4 h at 4 °C. The cell pellets were resuspended in lysis buffer (150 mM NaCl, 20mM tris, pH 8.0) and freeze-thawed three times. The deposit and lysate were mixed with MgCl<sub>2</sub> (1 mM) and Benzonase (250U/

mL, Sigma, USA) and homogenised completely. After centrifugation for 20 min at 5500 g, the supernatant was collected. Then virus was purified further through iodixanol gradients (17%, 25%, 40%, and 60%) at 240,000 g, 90 min, 16 °C. After centrifugation, the viral fraction in 40% was harvested and re-suspended in 1×PBS. The virus suspension was concentrated through 100 K columns at 3500 g, 30 min at 4 °C and aliquoted and stored at -80 °C. To evaluate the viral titre, AAV-293 cells were infected with the rAAV-gas6 at different dilutions and harvested for GAS6 assessment 48 h later.

### Intracerebroventricular injection of rAAV-gas6 or rAAV-GFP

Mice (4 weeks) were anesthetized using 10% chloral hydrate (0.1 ml/10 g body weight) and transferred to a stereotaxic apparatus (Stoelting Co., Wood Dale, IL, USA). Then, rAAV-gas6 or rAAV-GFP in 4 µl PBS was injected slowly (approximately 5 min) into cerebral ventricles (approximately 0.6 mm posterior to the bregma, 1.2 mm lateral right and 2.3 mm below dura) through a 5-µl microsyringe (Gaoche, China). GAS6 expression in the brain was tested by qPCR at 1, 2 and 3-weeks post-injection. Four weeks later, mice were subjected to JEV infection.

## Results

### Gas6 KO mice were more susceptible to JEV infection

GAS6 is a growth factor secreted by neurons, microglia, and endothelial cells in the CNS [11]. During JEV induced neuronal death, the mRNA of gas6 decreased (Supplementary Fig. 1A), and there was a negative correlation between gas6 expression and JEV copies in the brain (Supplementary Fig. 1B). The expression of gas6 decreased with neuronal loss (Supplementary Fig. 1C). GAS6 plays an important role in maintaining CNS homeostasis [12]. To explore the effect of gas6 expression on JE progression, gas6<sup>-/-</sup> and WT mice were peripherally infected with JEV at 10<sup>6</sup> PFU. Compared to WT mice, gas6<sup>-/-</sup> mice showed increased mortality (Fig. 1A), more serious behavioural scores (Fig. 1B), and weight loss (Fig. 1C) after JEV infection. At 3 dpi, the viral loads from the brains of most gas6<sup>-/-</sup> mice were higher than those of WT mice, which was accompanied by increased expression of CCL2, IL-1β, and IL-6 (Fig. 1D, E). At 5 dpi, there was a significant increase in the viral load (Fig. 1F) and proinflammatory cytokines including TNFα, CCL2, IFN γ, IL-1β, and IL-6 (Fig. 1G) in the gas6<sup>-/-</sup> group. Thus, gas6<sup>-/-</sup> mice were more susceptible to JEV infection indicating that GAS6 may be a protective factor against JEV infection.

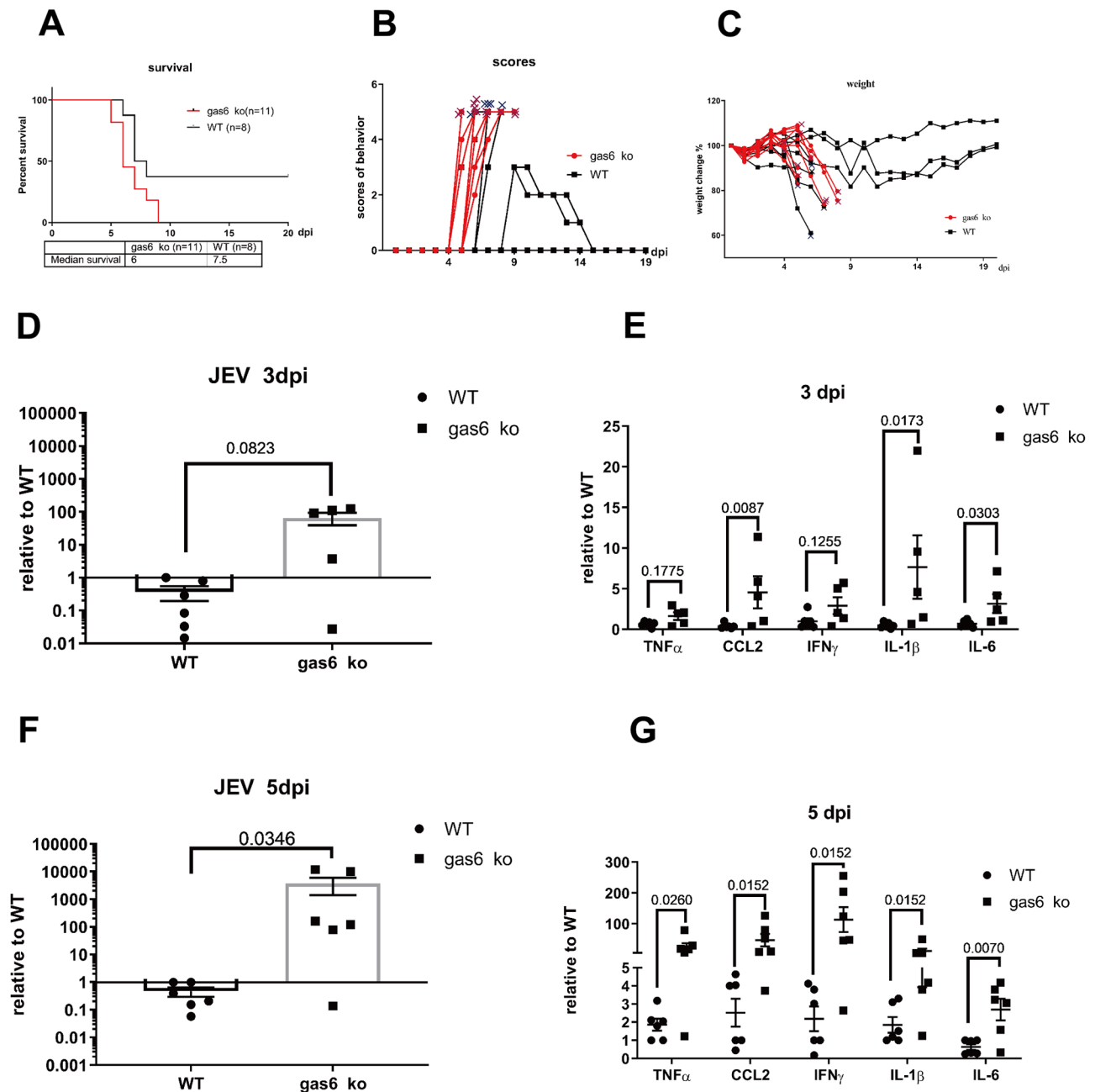


**Fig. 1** GAS6 KO mice were more susceptible to JEV infection peripherally. Gas6<sup>-/-</sup> and WT mice were infected with JEV at 10<sup>6</sup> PFU via foot pad injection. A, B, C. The survival rate (A), behavioural scores (B), and weight (C) of each group were recorded daily (gas6 ko n = 11; WT n = 8). D, F. The viral loads in gas6<sup>-/-</sup> and WT mouse brains at 3 dpi (D) and 5 dpi (F) were detected using qPCR (gas6<sup>-/-</sup> n = 5; WT n = 6). Data were normalised to  $\beta$ -actin and the relative change of viral copies was calculated based on the viral level of WT- d3- 1 or WT- d5- 1. Data are shown as mean  $\pm$  SD. E, G. Relative expression of proinflammatory cytokines (TNF- $\alpha$ , CCL2, IFN- $\gamma$ , IL-1 $\beta$ , IL-6) in gas6<sup>-/-</sup> and WT mouse brains at 3 dpi (E) and 5 dpi (G) were detected by qPCR (gas6<sup>-/-</sup> n = 5; WT n = 6). The data were normalised to  $\beta$ -actin and the relative change of expression was calculated based on the level of WT-d3-1 or WT-d5-1. Data are shown as mean  $\pm$  SD

**Mice with AXL, MERTK or AXL/MERTK blockage were vulnerable to JEV attack accompanied by aggravated neuroinflammation**

AXL and MERTK are the main GAS6 receptors with higher affinity than Tyro3 [5]. To identify whether the protective effects of GAS6 during JE occurred via AXL

or MERTK activation, AXL<sup>-/-</sup>, MERTK<sup>-/-</sup> or AXL/ MERTK (AM)- deleted mice were peripherally infected with JEV at different titres. At 10<sup>6</sup> PFU, 36% WT mice survived. All AXL<sup>-/-</sup>, MERTK<sup>-/-</sup> and AM<sup>-/-</sup> mice died. Meanwhile, the median survival time of AXL<sup>-/-</sup>, MERTK<sup>-/-</sup> and AM<sup>-/-</sup> mice were significantly shorter than that of

WT mice (Fig. 2A). Mice were infected with lower titre JEV at  $10^5$  PFU, and the survival proportion of  $AXL^{-/-}$ ,  $MERTK^{-/-}$  and  $AM^{-/-}$  mice were 6.67%, 0%, and 14.29%, respectively, which were still much lower than the survival proportion of the WT (38.46%) (Fig. 2B).

Collectively, mice with  $AXL$ ,  $MERTK$  or  $AM$  blockage were as vulnerable to JEV infection as  $GAS6$ -deficient mice.

$GAS6$  is the sole ligand of  $AXL$ , whereas  $MERTK$  and  $TYRO3$  are activated by  $PROS1$  in  $gas6$  KO mice [11]. The effects of  $GAS6$  signalling on JEV infection and

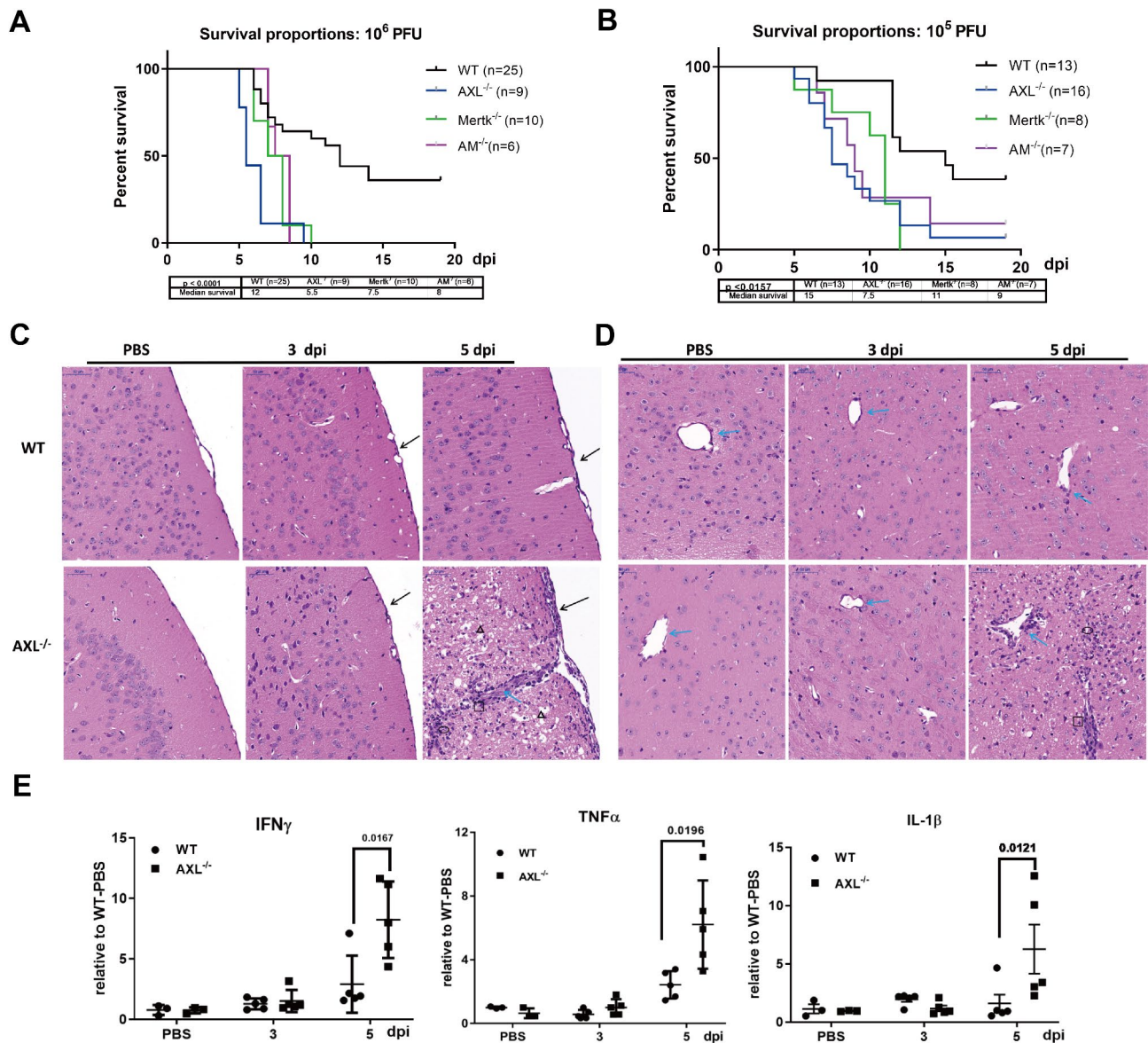


**Fig. 2**  $AXL$ ,  $MERTK$ , or  $AM$  deleted mice were vulnerable to JEV attack with aggravated neuroinflammation. **A**.  $AXL^{-/-}$ ,  $MERTK^{-/-}$ ,  $AM^{-/-}$ , and WT mice were infected with JEV at  $10^6$  PFU. The survival rates of  $AXL^{-/-}$ ,  $MERTK^{-/-}$  and  $AM^{-/-}$  mice were all 0%, and that of WT mice was 36%. The median survival times of  $AXL^{-/-}$ ,  $MERTK^{-/-}$ ,  $AM^{-/-}$ , and WT mice were 5.5, 7.5, 8, and 12 days respectively. **B**.  $AXL^{-/-}$ ,  $MERTK^{-/-}$ ,  $AM^{-/-}$ , and WT mice were infected with JEV at  $10^5$  PFU; the survival proportions of  $AXL^{-/-}$ ,  $MERTK^{-/-}$ , and  $AM^{-/-}$  mice were 6.67%, 0%, and 14.29%, while that of WT mice was 38.46%; the median survival times were 7.5, 11, 9, and 15 days, respectively.  $AXL^{-/-}$  and WT mice were infected with JEV at  $10^6$  PFU, and the brains from each group were harvested for HE staining and proinflammatory cytokine detection at 3 and 5 dpi. **C**. Histopathological changes in the meninges and cerebral cortex in each group. The meninges thickened after JEV infection, as indicated by the black arrows. There were obvious reticular softening lesions in the  $AXL^{-/-}$  mouse cortex, as indicated by black triangles at 5 dpi. **D**. The histomorphology of blood vessels in the brains of WT and  $AXL^{-/-}$  mice is indicated by blue arrows. Perivascular cuffing (blue arrow) and glial nodules (black squares) were more evident, and inflammatory cell accumulation (black circles) was increased in  $AXL^{-/-}$  mouse brains at 5 dpi. **E**. IFN- $\gamma$ , TNF- $\alpha$ , and IL-1 $\beta$  expression after JEV infection at 3 and 5 dpi was assayed by qPCR and was normalised to  $\beta$ -actin and the relative change was calculated based on the expression of cytokines in the brains of WT PBS- treated mice. PBS: WT  $n=3$ ,  $AXL^{-/-}$   $n=3$ ; 3 dpi: WT  $n=5$ ,  $AXL^{-/-}$   $n=5$ ; 5 dpi: WT  $n=5$ ,  $AXL^{-/-}$   $n=5$

neuroinflammation were explored in  $AXL^{-/-}$  mice. Histopathological changes and inflammatory cytokines in brains from WT and  $AXL^{-/-}$  mice were assayed at 3 and 5 dpi. Compared to the PBS treated groups, JEV infected mouse brains showed slightly thickened meninges at 3 dpi accompanied by infiltrated immune cells (Fig. 2C). At 5 dpi, there was a significant accumulation of inflammatory cells in the meninges and cortex, as well as more perivascular cuffings and glial nodules in  $AXL^{-/-}$  mice (Fig. 2D). As expected, proinflammatory cytokines including IFN- $\gamma$ , TNF- $\alpha$ , and IL-1 $\beta$  (Fig. 2E) were also increased significantly in  $AXL^{-/-}$  mouse brains at 5 dpi. Thus, the blockage of GAS6/AXL signaling accelerated neuroinflammation during JEV infection.

#### Deficiency of GAS6/AXL signal exacerbated BBB breakdown during JEV infection, which increased viral invasion into the CNS

In line with *gas6* KO mice, higher viral copy numbers (Fig. 3A) and JEV E protein levels were observed in  $AXL$  deleted mouse brains than that in WT mice at 3 and 5 dpi (Fig. 3B). We investigated the reasons of these differences. In the peripheral system, the level of infectious viral particles in  $AXL^{-/-}$  mouse blood was comparable to that in WT mice (SUP Fig. 2A) and was even lower at 3 dpi (SUP Fig. 2B). Meanwhile, there were no significant differences in IFN- $\beta$  expression (SUP Fig. 2D) and number of viral copies in the spleens between WT and  $AXL^{-/-}$  mice at 1 and 3 dpi (SUP Fig. 2C). To identify the effect of *gas6*/AXL signal on JEV propagation in the brains, intracerebral injection of JEV was performed in WT and  $AXL^{-/-}$  mice, and no significant difference in viral load was found at 1, 3 or 5 dpi (SUP Fig. 2E). These results showed that the *gas6*/AXL signal had little effect on JEV propagation in the peripheral system and brains. Thus, consistent with the results of Wang et al. [13], the blockage of *gas6*/AXL contributed to more viral particles entering into the brains during JEV peripheral infections. The BBB plays an important role in maintaining CNS homeostasis by preventing the invasion of pathogens. We next assessed the BBB integrity in WT and  $AXL^{-/-}$  mice.  $AXL^{-/-}$  mice showed increased EB leakage after JEV infection, especially at 5 dpi (Fig. 3C) which was consistent with *gas6* KO mice (SUP Fig. 2F). Meanwhile, NaF extravasation detection confirmed augmented BBB permeability in  $AXL^{-/-}$  mice compared to WT mice at 3 dpi (Fig. 3D). We next analysed the structure and expression of tight junction (TJ) proteins in the  $AXL^{-/-}$  and WT mouse brains. In  $AXL^{-/-}$  mouse brains, the continuity of ZO-1 expression decreased at 3 dpi, and the structures of ZO-1 and endothelial cells were significantly damaged at 5 dpi (Fig. 3E). Meanwhile, occludin expression was lower in  $AXL^{-/-}$  mouse brains at 3 dpi (Fig. 3F). Taken together, the BBB in GAS6/AXL blocked mice was more

liable to disruption, which allowed more viral particles to enter into the CNS.

#### GAS6 increased TJ proteins expression and BBB integrity in vitro

GAS6 has been reported to participate in maintaining the vascular endothelial barrier via AXL and MERTK by reinforcing TJ proteins [14, 15]. To explore the role of GAS6 in BBB maintenance during JEV infection, bEnd.3 cells were treated with the recombinant GAS6 protein (rGAS6). According to the cell proliferation assay, the viability of bEnd.3 cells treated with rGAS6 was comparable (Fig. 4A). The expression of claudin5 and occludin were relatively higher in rGAS6-treated bEnd.3 cells after JEV infection (Fig. 4B). In vitro BBB models were constructed using bEnd.3 cells combined with neuro2a and C8-D1A cells (Fig. 4C) and then treated with rGAS6 and JEV. The rGAS6-treated group showed higher TEER than the control, suggesting that GAS6 increased the integrity of bEnd.3 cell monolayer (Fig. 4D). TEER from  $AXL$  KO bEnd.3 cells decreased significantly after JEV infection, and rGAS6 treatment enhanced TEER partly indicating that other TAM receptors MERTK or TYRO3 also participated in BBB maintenance mediated by GAS6 (Fig. 4D). Thus, during JEV infection, GAS6 directly increased BBB integrity and TJ proteins expression in endothelial cells.

#### GAS6 supplementation increased BBB integrity in vivo

We investigated whether GAS6 over-expression in the brains strengthens the BBB in vivo. rAAV-*gas6* and rAAV-GFP were constructed, purified, and concentrated (SUP Fig. 3A, B). GAS6 expression was upregulated at 4 weeks after rAAV-*gas6* intracerebroventricular injection (SUP Fig. 3C). The distribution of rAAV was evaluated using AAV-GFP at 4 weeks after injection (SUP Fig. 3D). Mice overexpressing GAS6 or GFP were infected with JEV ( $10^7$  PFU) via the footpad. BBB permeability was detected at 5 dpi using EB staining (Fig. 5A) and NaF extravasation assay (Fig. 5B). Compared to the GFP group, the BBB integrity in the *gas6* group was increased. Meanwhile, the viral load in the CNS decreased at 3 (Fig. 5C) and 5 dpi (Fig. 5D) in the *gas6* group compared to that in the GFP group. Thus, GAS6 overexpression in the brains strengthened BBB and prevented viral invasion during JEV infection.

#### GAS6 alleviated neuroinflammation during JEV infection

To determine whether GAS6 overexpression affected neuroinflammation, changes in cytokine levels and histopathology in both the *gas6* and GFP groups were detected after JEV infection. Even though the difference was not statistically significant, CCL2, TNF $\alpha$ , IL-1 $\beta$  (Fig. 6A, B, C) expression was lower in most of the brains with GAS6 overexpression compared to those of the GFP

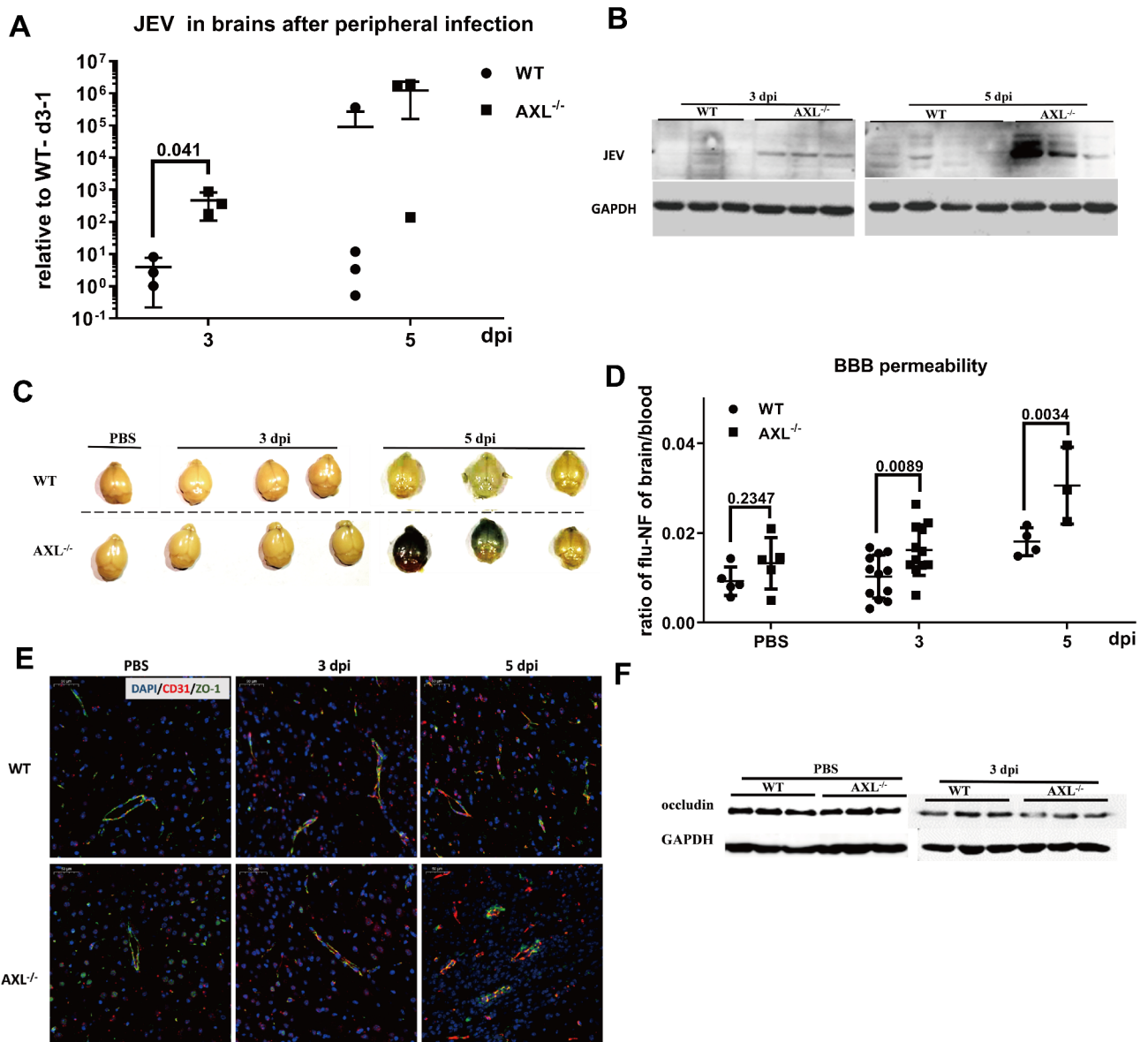


**Fig. 3** Deficiency of GAS6/AXL signal exacerbated BBB breakdown during JEV infection. WT and  $AXL^{-/-}$  mice were infected with JEV  $10^6$  PFU via foot pad. **A** Viral copies in each brain sample were tested by qPCR. Data were normalized to  $\beta$ -actin and the relative change was calculated based on the viral level of WT-d3-1. At 3 dpi, WT  $n=3$ ,  $AXL^{-/-}n=3$ ; at 5 dpi, WT  $n=4$ ,  $AXL^{-/-}n=3$ . Data are shown as mean  $\pm$  SD. **B** The JEV E protein in the brain was detected by WB. At 3 dpi, WT  $n=3$ ,  $AXL^{-/-}n=3$ ; at 5 dpi, WT  $n=4$ ,  $AXL^{-/-}n=3$ . **C** Qualitative detection of BBB permeability via EB staining at 3 and 5 dpi. **D** Quantitative assay of BBB permeability using NaF extravasation. NaF leakage was calculated based on the fluorescence ratio in the brain to blood. PBS: WT  $n=5$ ,  $AXL^{-/-}n=3$ ; 3 dpi: WT  $n=12$ ,  $AXL^{-/-}n=12$ ; 5 dpi: WT  $n=4$ ,  $AXL^{-/-}n=3$ . The data represent the mean  $\pm$  SD. **E** Representative images show the co-localisation of endothelial cells (CD31, red) and tight junction proteins (ZO-1, green) in the brains of WT and  $AXL^{-/-}$  mice at 3 and 5 dpi. Compared to WT mice, the expression of ZO-1 and CD31 in  $AXL^{-/-}$  mouse brains showed a slight discontinuity at 3 dpi. At 5 dpi, the structures of CD31 and ZO-1 were much fuzzier in  $AXL^{-/-}$  mouse brains than in WT mice. **F** Expression of the tight junction protein occludin in WT and  $AXL^{-/-}$  mouse brains at 3 dpi (PBS treated WT  $n=3$ ,  $AXL^{-/-}n=3$ ; JEV treated WT  $n=3$ ,  $AXL^{-/-}n=3$ )

group during JEV infection. Meanwhile, meningitis and inflammatory cells infiltration were alleviated in *gas6*-mouse brains compared to GFP-mice at 5 dpi (Fig. 6D). In addition, there were few perivascular cuffings and glial nodules in the *gas6*-mouse brains but not in the GFP group (Fig. 6E). Thus, the alleviated neuroinflammation in *GAS6*-overexpressed mice during JEV infection might

be due to enhanced BBB integrity which prevented JEV and inflammatory cells from entering the CNS, as well as immunoregulation of *GAS6*, which has been reported to regulate glia activation and inhibit neuroinflammation [12].

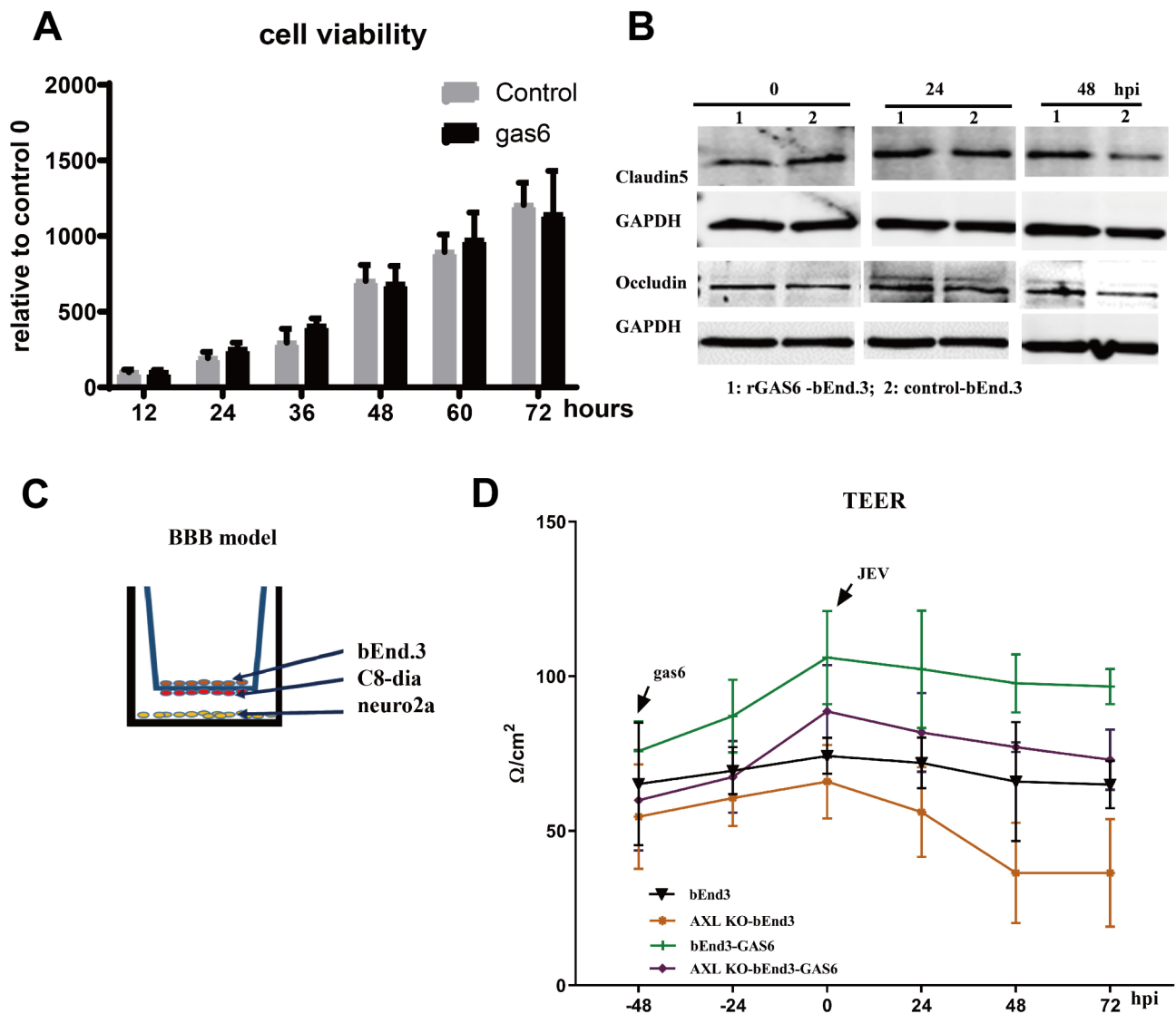


**Fig. 4** GAS6 increased TJ protein expression and BBB integrity in vitro. **A**. Proliferation activity of bEnd.3 cells treated with GAS6 or serum free culture medium. **B**. bEnd.3 (cultured with media or media containing rGAS6) were treated with a homogenate supernatant from JEV- infected mouse brains. Expression of TJ proteins, including claudin5 and occluding, at 24 and 48 hpi. **C**. Schematic diagram of the in vitro BBB model constructed using bEnd.3, C8-dia and neuro2a cells in a Transwell system. **D**. In BBB models, neuro2a cells were infected with JEV, bEnd.3 cells were treated with media alone or media containing rGAS6. TEER was detected in all groups. The TEER in rGAS6 treated bEnd.3 cells was higher than that in the other groups

**Mice supplemented with GAS6 in brains were more resistant to JEV infection**

We next explored whether GAS6 overexpression decreased morbidity and mortality induced by JEV infection. When infected with JEV at a relatively low titre ( $10^7$  PFU), gas6- mice showed alleviated weight loss (Fig. 6A) and symptom score (Fig. 6B) as well as decreased mortality (Fig. 6C) compared to the GFP- mice. At  $2 \times 10^7$  PFU, most of the gas6- mice showed delayed onset of JE (Fig. 6D, E) and improved behavioural scores (Fig. 6F). When infected with a higher dose ( $3 \times 10^7$  PFU), several mice in the gas6- group survived, with a total survival time that was longer than that of GFP mice, which were all sacrificed (Fig. 6G, H, I). In general, GAS6

supplementation in mouse brains alleviated JE progression (See Fig 7).

**Discussion**

Viral encephalitis is a potentially fatal sequela of viral infection across the globe. The common pathogenic characteristics of viral encephalitis are frequently associated with BBB disruption, enabling viruses, inflammatory cells, and deleterious molecules to enter the brain parenchyma [16]. In this study, we found that GAS6 was downregulated in the brains of JE models, which was accompanied by increased BBB leakage. Mice with GAS6 blockage or AXL, and MERTK deletion were more susceptible to JEV infection, which was accompanied by

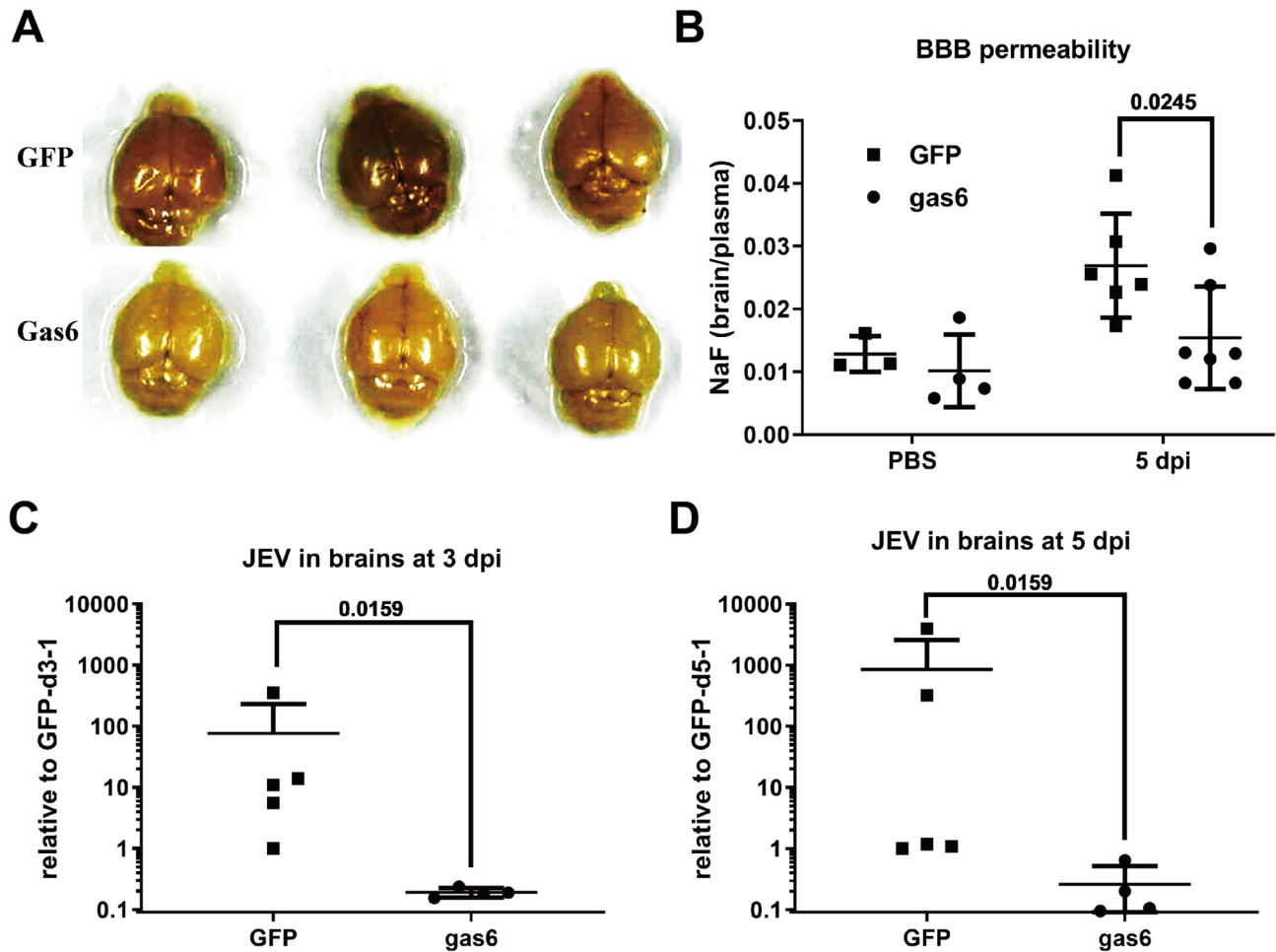


**Fig. 5** Gas6 Supplementation increased BBB integrity in vivo. Recombinant AAV-gas6 (rAAV-gas6) or rAAV-GFP was constructed and intracerebroventricularly injected into the mouse brains. Four weeks after rAAV-gas6 or rAAV-GFP injection, the mice were infected with JEV via the foot pad ( $10^7$  PFU). (GFP: rAAV-GFP injected mice; gas6: rAAV-gas6 injected mice) **A**. Qualitative detection of BBB permeability by EB leakage into brains at 5 dpi. **B**. Quantitative assay of BBB permeability via NaF extravasation at 5 dpi (Data represent mean  $\pm$  SD). **C, D**. Viral copies in the brains of each group at 3 and 5 dpi were tested using qPCR. Data were normalised to  $\beta$ -actin and the relative change of viral copies was calculated based on the viral level of GFP-d3-1 (C) or GFP-d5-1 (D). Data are shown as mean  $\pm$  SD

more serious neuroinflammation and BBB breakdown. GAS6 overexpression in brains improved BBB integrity and enhanced resistance to peripheral JEV infection.

MERTK and AXL maintain BBB integrity during WNV infection [15]. Additionally, it has been reported that AXL-deleted macrophages secreted more IL-1 $\alpha$  which promoted BBB breakdown during JEV infection [13]. In this study, we found that both MERTK and AXL showed protective effects against JEV invasion and that MERTK and AXL in endothelial directly enhanced BBB integrity. Meanwhile, we found that deficiency in GAS6, the ligand of TAM receptors, aggravated JE progression and that mice with gas6 overexpression in the brain showed increased resistance to JEV infection. Furtherly, the different role of GAS6 interaction with MERTK, AXL and Tyro3 are being explored in our lab.

GAS6 contributed to maintenance of CNS homeostasis by binding to TAM receptors including Tyro3, AXL and MERTK. Currently, it is thought that GAS6 is the sole ligand to AXL. Therefore, AXL KO mice were mainly used to identify the effect of blocking GAS6/AXL signaling on JE progression in this study. It has been reported that AXL mediated viral entry into glial cells and inhibited innate immune responses during ZIKV infection [17]. However, in the present study, the effect of AXL on JEV propagation in the brain was not significant. Indeed, our group revealed that AXL-deleted neurons promoted JEV infection by dampening innate immunity [7]. JEV NS2B-3 protein complex down-regulated AXL expression to promote cell apoptosis and viral particle release [18]. Thus, GAS6/ AXL may provide comprehensive protection by strengthening BBB integrity, activating cellular

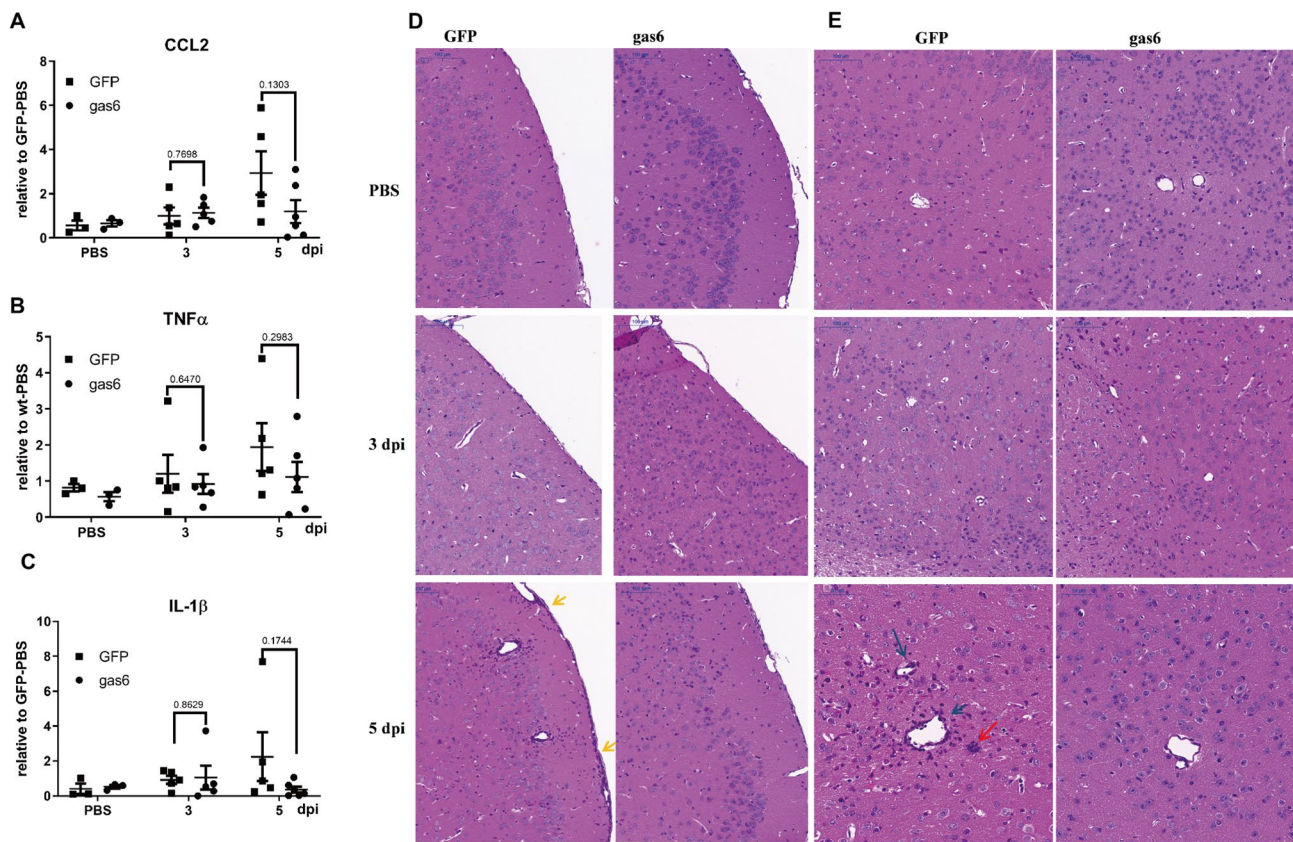


**Fig. 6** GAS6 alleviated neuroinflammation during JEV infection. The brains from gas6 or GFP mice were harvested for cytokines detection and HE staining at 3 and 5 dpi. **A. B. C.** The expression of CCL2 (A), TNF $\alpha$  (B), IL-1 $\beta$  (C) were detected by qPCR. Data were normalised to  $\beta$ -actin and the relative change was calculated based on the level in PBS treated mouse brains. Data represent the mean  $\pm$  SD. **D.** Histopathological changes in the meninges and cerebral cortex in the GFP group were significantly thickened, accompanied by infiltrated inflammatory cells at 5 dpi (yellow arrows), which were alleviated in the gas6 group. **E.** Histomorphology of blood vessels in the brains of GFP and gas6 groups. Increased inflammatory cell accumulation around vessels (blue arrows) and glial nodules (red arrow) was observed in GFP mouse brains, but not in gas6 mouse brains at 5 dpi

innate immunity and limiting viral particles release during JEV infection.

During JEV infection, the initiation of BBB breakdown is complicated, and the aggravation of BBB permeability amplifies secondary neuroinflammation [19]. After evasion from peripheral immunity, JEV enters into CNS via intricate pathways such as transcytosis of brain endothelial cells, peripheral-infected leukocytes mediated “Trojan horse”, and direct infection of peripheral axons and olfactory bulb [4]. Direct damage to endothelial cells from JEV infection has a negligible effect on the breakdown of BBB. Indeed, it has been demonstrated that entry of JEV into the CNS occurs earlier than BBB breakdown [20]. Moreover, previous studies demonstrated that the inflammatory cytokines, such as IFN  $\gamma$ , TNF $\alpha$ , CXCL10, and chymase, released by JEV-infected innate immune cells in the CNS promoted BBB breakdown [21, 22]. GAS6-enhanced BBB integrity may be mediated by directly increasing endothelial function and regulating neuroinflammation [23]. Massive neuronal death and loss may lead to decreased GAS6 production and impaired

GAS6/ TAM signals during JEV infection. Meanwhile, downregulation of GAS6 augmented BBB compromise, which allowed more viral particles to enter CNS, leading to increased neuronal death. Therefore, GAS6 Supplementation may alleviate this vicious cycle.

Supplementing the brain with GAS6 is a potential strategy for JE treatment. In this study, rAAV-GAS6 was constructed and injected into the lateral ventricles to achieve overexpression in the brains. We attempted to directly deliver rGAS6 protein into the brains after JEV infection. However, continuous intracerebral pumping was difficult to perform, and few mice survived surgery. Next, we will explore vehicles to achieve CNS-targeted delivery from the peripheral system.

GAS6/TAM signalling alleviates neuroinflammation by regulating microglia and promotes neurogenesis by supporting neural stem cells (NSCs) [11, 24]. Additionally, GAS6/TAM signalling contributes to the survival of oligodendrocytes and improved remyelination [24]. In this study, we focused on the role of GAS6 in BBB integrity and neuroinflammation. Because GAS6/TAM signals

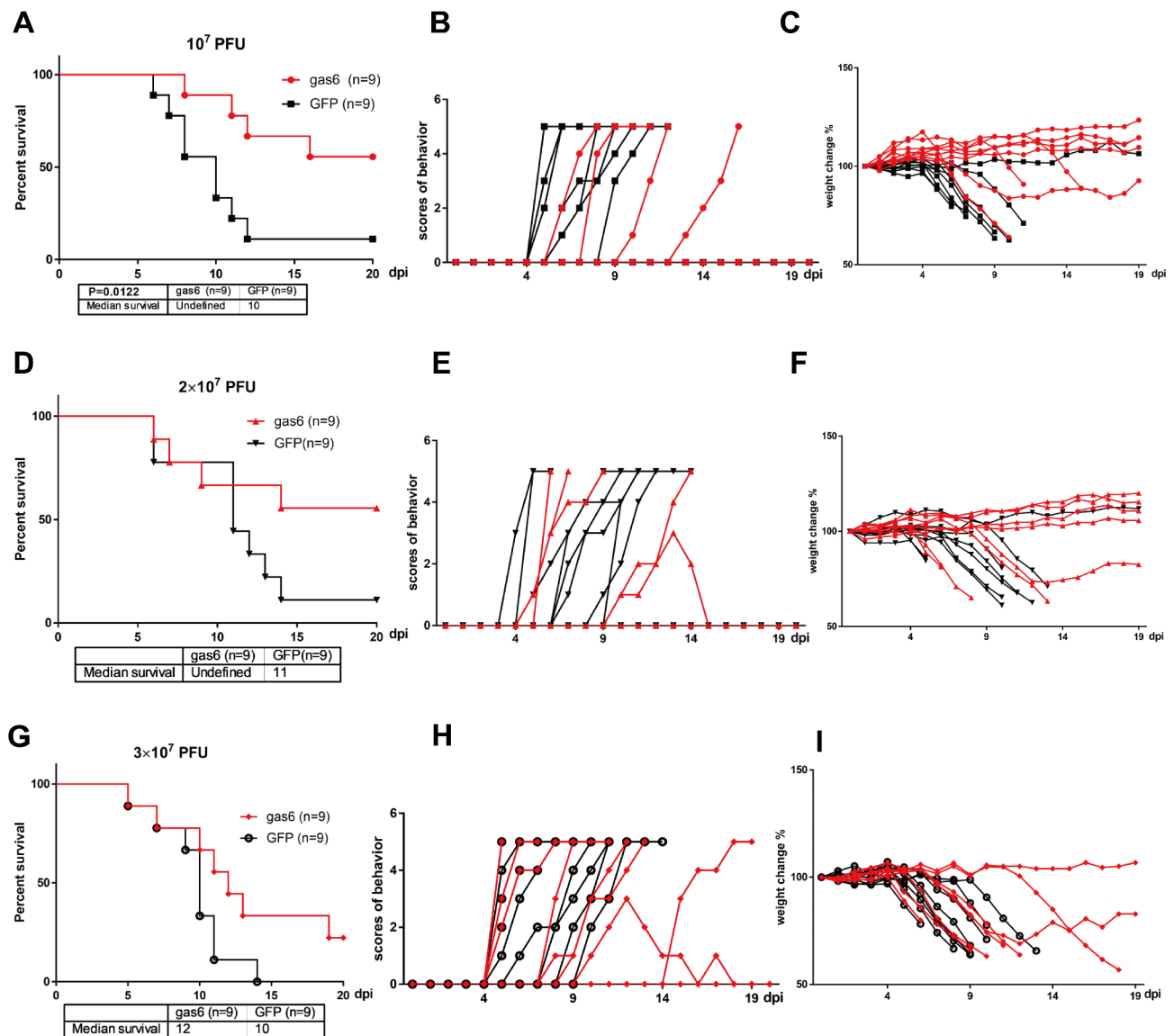


**Fig. 7** Mouse brains supplemented with GAS6 were more resistant to JEV infection. Gas6 and GFP mice were infected with JEV at different MOIs via foot pad injection, and survival changes, behavioural scores, and weights in each group were recorded daily. **A, B, C.** Survival rates of gas6 and GFP mice infected with JEV at  $10^7$  PFU were 55.56% and 11.11%, respectively. The median survival time of the GFP mice was 10 days (left). The behavioural scores (B) and body weights (C) of each mouse were recorded until death. **D, E, F.** Survival rates of gas6 and GFP mice infected with JEV at  $2 \times 10^7$  PFU were 55.56% and 11.11%, respectively. The median survival time of GFP mice was 11 days (left). The behavioural scores (E) and body weights (F) of each mouse were recorded until death. **G, H, I.** Survival rates of gas6 and GFP mice infected with JEV at  $3 \times 10^7$  PFU were 22.22% and 0% respectively. The median survival times of the gas6 and GFP mice were 12 and 10 days, respectively. The behavioural scores (H) and body weight (I) of each mouse were recorded until death

promote microglial phagocytosis of apoptotic cells and myelin debris, increases oligodendrogenesis and myelination, and supports neuronal survival [25], the role of GAS6 in improving neurological sequelae requires further investigation.

In conclusion, GAS6 played a protective role against the progression of JE. GAS6 overexpression enhanced BBB integrity and resistance to JEV invasion and neuroinflammation. Our study suggested that GAS6 supplementation is a potential therapeutic strategy for JEV

infections and other types of viral encephalitis. This finding has promising prospects because of the expansion of elderly populations with increased BBB degeneration, who are more susceptible to viral infections [26].

**Abbreviations**

- AAV Adeno associated virus
- AXL AXL receptor tyrosine kinase
- BBB Blood brain barrier
- BHK Baby hamster kidney
- CCL2 C-C motif chemokine ligand 2
- CNS Central nervous system

DAMPs	Damage associate molecule patterns
Dpi	Days post-infection
EB	Evans Blue
FBS	Fetal bovine serum
GAS6	Growth-arrest specific gene 6
HE	Hematoxylin–eosin
IHC	Immunohistochemical
IFN $\gamma$	Interferon- $\gamma$
IL-1 $\beta$	Interleukin- 1 $\beta$
IL-6	Interleukin- 6
JE	Japanese encephalitis
JEV	Japanese encephalitis virus
KO	Knock out
MerTK	MER proto-oncogene tyrosine kinase
PFA	Paraformaldehyde
PFU	Plaque forming unit
rAAV-gas6	Recombinant AAV-gas6
RIPA buffer	Radio Immunoprecipitation Assay Lysis buffer
TAM	Tyro3, Axl, and MerTK
TJ	Tight junction
TNF $\alpha$	Tumor necrosis factor $\alpha$
WT	Wild type
ZO-1	Zonula occluden-1

## Supplementary Information

The online version contains supplementary material available at <https://doi.org/10.1186/s12974-024-03225-1>.

**Supplementary Material 1:** Supplementary fig 1. GAS6 was decreased in JEV-infected brains and was correlated reversely with viral load. A. Mice were infected with JEV (107 PFU) via peripheral injection, and their brains were harvested at 3 and 5 dpi. The expression of GAS6 in the brains was detected by qPCR. Data were normalised to  $\beta$ -actin and the relative change was calculated based on the level in PBS treated mouse brains. Data represent the mean  $\pm$  SD (PBS n = 6; 3 dpi n = 8; 5 dpi n = 6). B. Correlation analysis of GAS6 expression and JEV copies in JEV- infected brains. C. Immunofluorescence staining showing the expression of JEV E protein (red) and GAS6 (green) in JEV- infected brains

**Supplementary Material 2:** Supplementary fig 2. Viral load in WT and AXL $^{-/-}$  mice after intracerebral or peripheral JEV infection. WT and AXL $^{-/-}$  mice were injected with PBS or JEV 106 PFU via the footpad, spleen and the plasma from each mouse were harvested at 1 and 3 dpi (1 dpi: WT n = 3, AXL $^{-/-}$  n = 4; 3 dpi: WT n = 4, AXL $^{-/-}$  n = 4). A, B. Infectious JEV particles in the blood of WT and AXL $^{-/-}$  mice at 1 (A) and 3 dpi (B) were detected by plaque assay. C. The viral load in the spleens of WT and AXL $^{-/-}$  mice at 1 and 3 dpi was assayed by qPCR. Data were normalised to  $\beta$ -actin and the relative change of viral copies was calculated based on the viral level of WT-d1-1. PBS: WT n = 3, AXL $^{-/-}$  n = 3; 1 dpi: WT n = 3, AXL $^{-/-}$  n = 4; 3 dpi: WT n = 4, AXL $^{-/-}$  n = 4. Data are shown as the mean  $\pm$  SD. D. IFN- $\beta$  in spleens of WT and AXL $^{-/-}$  mice was assayed by qPCR. Data were normalised to  $\beta$ -actin and the relative change was calculated based on the level in WT-PBS. E. Viral copies in the brains of WT and AXL $^{-/-}$  mice at 1, 3, and 5 dpi after intracerebral injection of 100 PFU of JEV were detected by qPCR. Data were normalised to  $\beta$ -actin and the relative change of viral copies was calculated based on the viral level of WT-d1-1. At 1 dpi: WT n = 4, AXL $^{-/-}$  n = 5; 3 dpi: WT n = 3, AXL $^{-/-}$  n = 3; 5 dpi: WT n = 4, AXL $^{-/-}$  n = 4. Data are shown as the mean  $\pm$  SD. F. WT and gas6 $^{-/-}$  mice were infected with JEV 106 PFU via the footpad. Qualitative detection of BBB permeability using EB staining at 4 dpi

**Supplementary Material 3:** Supplementary fig 3. Preparation and identification of rAAV-gas6 in vitro and in vivo. A. Schematic diagram of recombinant pAAV-gas6. B. Concentration, purification and identification of rAAV-gas6. AAV-293 cells were infected with supernatant from the AAV-packaged system, concentrated virus diluted at 1: 103; 1: 104; 1: 105 and supernatant after ultracentrifugation. After 48 h, the GAS6 expression in each group was detected using qRT-PCR. C, D. rAAV-gas6 was constructed and injected intracerebroventricularly into the mouse brain. C. Expression of GAS6 in the brains at 1, 2, and 3 weeks after intracerebroventricular injection. The relative expression of GAS6 in the mouse brain increased after rAAV-gas6 injection. Data represent the mean  $\pm$  SD. D. Distribution of

GFP 4 weeks post rAAV-GFP intracerebroventricular injection (1. rAAV-GFP injection; 2. PBS injection)

Supplementary Material 4

Supplementary Material 5

## Acknowledgements

We would like to thank Professor Daishu Han (Institute of Basic Medical Sciences, Peking Union Medical College–Chinese Academy of Medical Sciences) for providing AXL and MerTK knockout mice for this study.

## Author contributions

BPY, ZHJ, YCT performed most of the experiments and prepared the manuscript; LCY, JH, WY, DYC, YJ contributed to construction of JE models, rAAV-gas6 and analysis of data. ZFL, WXM contributed to the conception of this study and resources. ZY and JZS contributed to interpretation of data, manuscript preparation and revision. LYF contributed to the conceptualization, resources, supervision, writing and funding acquisition.

## Funding

This work was supported by the National Natural Science Foundation of China (No. 81871697).

## Data availability

No datasets were generated or analysed during the current study.

## Declarations

### Ethics approval and consent to participate

All animal experiments were reviewed and approved by the Animal Care and Use Committee of the Laboratory Animal Center, Air Force Medical University. The number of Animal Experimental Ethical Inspection is 20160112.

### Consent for publication

Not applicable.

### Competing interests

The authors declare no competing interests.

Received: 19 March 2024 / Accepted: 5 September 2024

Published online: 19 September 2024

## References

- Japanese encephalitis - World Health Organization [Internet]. 2019. <https://www.who.int/news-room/fact-sheets/detail/japanese-encephalitis>
- Zhang S, Hu W, Qi X, Zhuang G. How Socio-Environmental factors are Associated with Japanese Encephalitis in Shaanxi, China-A bayesian spatial analysis. *Int J Environ Res Public Health*. 2018;15:608.
- Lannes N, Summerfield A, Filgueira L. Regulation of inflammation in Japanese encephalitis. *J Neuroinflammation*. 2017;14:158.
- Mustafá YM, Meuren LM, Coelho SVA, de Arruda LB. Pathways exploited by flaviviruses to counteract the blood-brain barrier and invade the Central Nervous System. *Front Microbiol*. 2019;10:525.
- van der Meer JHM, van der Poll T, van 't Veer C. TAM receptors, Gas6, and protein S: roles in inflammation and hemostasis. *Blood*. 2014;123:2460–9.
- Wang Z-Y, Zhen Z-D, Fan D-Y, Wang P-G, An J. Axl alleviates Neuroinflammation and Delays Japanese Encephalitis Progression in mice. *Virology*. 2021;36:667–77.
- Yang J, Li M, Yuan M, Bian P, Dong Y, Zhang H, et al. Axl $^{-/-}$  neurons promote JEV infection by dampening the innate immunity. *Virus Res*. 2022;307:198605.
- Gruber RC, Ray AK, Johndrow CT, Guzik H, Burek D, de Frutos PG, et al. Targeted GAS6 delivery to the CNS protects axons from damage during experimental autoimmune encephalomyelitis. *J Neurosci*. 2014;34:16320–35.
- Tsugawa H, Ohki T, Tsubaki S, Tanaka R, Matsuzaki J, Suzuki H, et al. Gas6 ameliorates intestinal mucosal immunosenescence to prevent the translocation of a gut pathobiont, *Klebsiella pneumoniae*, to the liver. *PLoS Pathog*. 2023;19:e1011139.

10. Bian P, Zheng X, Wei L, Ye C, Fan H, Cai Y, et al. MLKL mediated necroptosis accelerates JEV-Induced Neuroinflammation in mice. *Front Microbiol.* 2017;8:303.
11. Fourgeaud L, Través PG, Tufail Y, Leal-Bailey H, Lew ED, Burrola PG, et al. TAM receptors regulate multiple features of microglial physiology. *Nature.* 2016;532:240–4.
12. Shafit-Zagardo B, Gruber RC, DuBois JC. The role of TAM family receptors and ligands in the nervous system: from development to pathobiology. *Pharmacol Ther.* 2018;188:97–117.
13. Wang Z-Y, Zhen Z-D, Fan D-Y, Qin C-F, Han D-S, Zhou H-N, et al. Axl Deficiency promotes the neuroinvasion of Japanese Encephalitis Virus by enhancing IL-1 $\alpha$  production from Pyroptotic Macrophages. *J Virol.* 2020;94:e00602–20.
14. Ni J, Lin M, Jin Y, Li J, Guo Y, Zhou J, et al. Gas6 attenuates Sepsis-Induced tight Junction Injury and vascular endothelial hyperpermeability via the Axl/NF- $\kappa$ B signaling pathway. *Front Pharmacol.* 2019;10:662.
15. Miner JJ, Daniels BP, Shrestha B, Proenca-Modena JL, Lew ED, Lazear HM, et al. The TAM receptor Mertk protects against neuroinvasive viral infection by maintaining blood-brain barrier integrity. *Nat Med.* 2015;21:1464–72.
16. Xj DY, Dz L, Xi T. L, B W. Advances in viral encephalitis: Viral transmission, host immunity, and experimental animal models. *Zoological research [Internet].* 2023 [cited 2024 Mar 14];44. <https://pubmed.ncbi.nlm.nih.gov/37073800/>
17. Chen J, Yang Y-F, Yang Y, Zou P, Chen J, He Y, et al. AXL promotes Zika virus infection in astrocytes by antagonizing type I interferon signalling. *Nat Microbiol.* 2018;3:302–9.
18. Xie S, Liang Z, Yang X, Pan J, Yu D, Li T, et al. Japanese Encephalitis Virus NS2B-3 protein complex promotes cell apoptosis and viral particle release by Down-regulating the expression of AXL. *Viol Sin.* 2021;36:1503–19.
19. Sharma KB, Vrati S, Kalia M. Pathobiology of Japanese encephalitis virus infection. *Mol Aspects Med.* 2021;81:100994.
20. Li F, Wang Y, Yu L, Cao S, Wang K, Yuan J, et al. Viral infection of the Central Nervous System and Neuroinflammation Precede blood-brain barrier disruption during Japanese encephalitis virus infection. *J Virol.* 2015;89:5602–14.
21. Hsieh JT, Rathore APS, Soundarajan G, St John AL. Japanese encephalitis virus neuropenetration is driven by mast cell chymase. *Nat Commun.* 2019;10:706.
22. Wang K, Wang H, Lou W, Ma L, Li Y, Zhang N, et al. IP-10 promotes blood-brain barrier damage by Inducing Tumor Necrosis Factor Alpha Production in Japanese encephalitis. *Front Immunol.* 2018;9:1148.
23. Wang Z-Y, Wang P-G, An J. The multifaceted roles of TAM receptors during viral infection. *Viol Sin.* 2021;36:1–12.
24. Gely-Pernot A, Coronas V, Harnois T, Prestoz L, Mandairon N, Didier A, et al. An endogenous vitamin K-dependent mechanism regulates cell proliferation in the brain subventricular stem cell niche. *Stem Cells.* 2012;30:719–31.
25. Goudarzi S, Rivera A, Butt AM, Hafizi S. Gas6 promotes oligodendrogenesis and myelination in the adult Central Nervous System and after Lysolecithin-Induced demyelination. *ASN Neuro.* 2016;8:1759091416668430.
26. Knox EG, Aburto MR, Clarke G, Cryan JF, O'Driscoll CM. The blood-brain barrier in aging and neurodegeneration. *Mol Psychiatry.* 2022;27:2659–73.

### Publisher's note

Springer Nature remains neutral with regard to jurisdictional claims in published maps and institutional affiliations.